Rare-earth minerals yttrian zirconolite and allanite-(Ce)* and associated minerals from Koberg mine, Bergslagen, Sweden

M. A. ZAKRZEWSKI, W. J. LUSTENHOUWER, H. J. NUGTEREN

Institute of Earth Sciences, Free University, De Boelelaan 1085, 1081 HV Amsterdam, The Netherlands

AND

C. T. WILLIAMS

Department of Mineralogy, The Natural History Museum, Cromwell Road, London SW7 5BD, U.K.

Abstract

A study of mine dump material from Koberg, Bergslagen, Sweden has revealed a varied mineral assemblage, including Zr-, *REE*-, Th- and U-bearing minerals associated with the sulphide ore deposit. Detailed descriptions and microprobe analyses are presented of the rare earth minerals yttrian zirconolite and allanite-(Ce), and the zirconium oxide baddeleyite. Yttrian zirconolite is patchily zoned in the actinide elements Th and U, and the low analytical totals suggest the presence of several weight per cent of H_2O. The implications of these features with respect to synthetic zirconolite in SYNROC and to radioactive waste management are briefly discussed. Chemical zoning of individual *REE* in yttrian zirconolite is described and the *REE* distribution compared with those of zirconolites from other localities. Allanite-(Ce) is generally unzoned, but contains *REE*-rich rims which are considered to be sub-micron intergrowths of allanite plus a bastnäsite-type mineral phase. The MgO content of allanite-(Ce) is unusually high and appears to be a characteristic feature of allanite from other cerium and mineral occurrences of Central Sweden. The rare earth minerals at Koberg are interpretated as having been formed as a result of localized remobilization of elements including Ti and Zr with H_2O- and CO_2-rich fluids.

KEYWORDS: zirconolite, allanite-(Ce), dissakisite-(Ce), baddeleyite, Koberg mine, Bergslagen, Sweden, rare earth minerals, zincian spinel, titanian clinohumite, metacarbonates, skarn.

Introduction

THE disused Pb–Zn mine at Koberg is situated approximately 10 km east of the town of Filipstad in Western Bergslagen, central Sweden (59°43′N 14°15′E). The deposit was discovered in 1730 where it was first worked for silver from Ag-bearing galena, and later in 1915 for zinc ore (Tegengren, 1924). The ore body contained sphalerite and galena in lenses up to 0.5 m thick and 5–10 m long within limestone, the whole deposit being confined to a lens of marble skarn interbedded within a rhyolitic metavolcanic sequence of Precambrian age (approximately 1.8 Ga). It is widely accepted (e.g. Baker *et al.*, 1988) that the sulphide occurrences of the Koberg type in Bergslagen originated by exhalative–sedimentary processes. Regional metamorphism and associated metasomatic processes remobilized many of the elements within the volcano–sedimentary pile (Rickard, 1988), and gave rise to the present day distribution of the ore body.

Although the mine is no longer accessible, on the mine dumps the most common rock types to be found are a pure white limestone marble, a light-green coloured skarn material, and intergrowths of these two types. Less common are blocks of dolomite, diabase, mica-rich fracture filling 'sköl' (an alteration product consisting of almost pure biotite, muscovite, chlorite, ±talc and minor cordierite, almandine and anthophyllite; Gavelin, 1989) and sulphide ore.

Here, we report the results of an optical and electron microprobe study of samples from the mine dumps: we describe the mineralogical and chemical characteristics of two rare earth min-

* Similar to new mineral dissakisite-(Ce); See Addendum, p. 35.

Mineralogical Magazine, March 1992, Vol. 56, pp. 27–35

erals identified in the samples, yttrian zirconolite and allanite-(Ce), and compare the material with the cerium mineral occurrences of the Bastnäs type in central Sweden.

Mineralogy

Igelström (1871) identified chondrodite, epidote, chlorite, tremolite, muscovite, magnetite, serpentine and ghanite from the marble skarn and associated rocks. In this investigation we identified additionally dolomite, olivine, phlogopite, titanian clinohumite (with 1.35% TiO_2), zircon, garnet (pyrope$_{60}$ almandine$_{40}$), zincian spinel ($Zn_{0.5}Mg_{0.4}Fe_{0.1}Al_2O_4$), apatite (not analysed), baryte, baddeleyite, and rare earth minerals yttrian zirconolite and allanite-(Ce)—the last three minerals are described in more detail below. Opaque minerals found in ore samples from the dumps include abundant sphalerite with up to 8 wt.% Fe, 0.4 wt.% Mn and 0.15% Cd, galena with Sb, Bi, Ag and Se below the detection limit of the wavelength-dispersive microprobe (i.e. less than 0.03 to 0.06 wt%), arsenopyrite, pyrrhotite and pyrite. Less abundant are chalcopyrite and bornite. Accessory minerals present are magnetite ($Fe^{3+}{}_{1.95}Al_{0.02}V_{0.03}Fe^{2+}{}_{0.96}$ $Mg_{0.04}O_4$), manganoan ilmenite ($Fe_{0.5}Mn_{0.4}$ $Mg_{0.1}TiO_3$), hematite, marcasite, molybdenite, covellite, cubanite, chalcocite, tetrahedrite, and graphite.

Baddeleyite, essentially ZrO_2, is a relatively rare mineral that occurs as an accessory in gabbro sills, diabase dykes, kimberlites, some alkaline rocks and carbonatites, and is concentrated also as placer deposits (see e.g. Purtscheller and Tessardi, 1985). In some occurrences the mineral is associated with zirconolite. More rarely is baddeleyite associated with both zirconolite and zircon (all three are major Zr-bearing minerals) as was observed in this study. In Koberg, baddeleyite occurs as euhedral to subhedral grains, up to 250 μm in size, intergrown with sphalerite and galena in the mineralized skarn.

The optical properties of baddeleyite in reflected light are very similar to those of sphalerite, and in isolated grains can be misidentified as sphalerite. In direct contact with sphalerite, baddeleyite by comparison has a slightly lower reflectivity, and displays yellow internal reflections in contrast to the dark brown reflections of sphalerite. Weak anisotropy of baddeleyite is only perceptible along grain boundaries.

Microprobe analyses of the Koberg baddeleyite show only minor amounts of Hf replacing Zr. Analyses of two grains gave respectively: ZrO_2 wt.% 98.1 (grain 1, core), 98.5 (grain 1, rim), 98.4 (grain 2) and HfO_2 wt.% 1.15, 1.17, 1.27 with FeO and TiO_2 below the level of 0.1%. This composition is typical for terrestrial baddeleyites (in contrast to lunar baddeleyites where Hf, Fe and Ti values are significantly higher; Frondel, 1975).

Yttrian zirconolite. The name zirconolite is used here for a mineral with composition close to $CaZrTi_2O_7$ with structures not determined, and is in accordance with the IMA nomenclature procedure given by Bayliss *et al.*, 1989.

The zirconolite occurs in a sample of 'sköl' consisting of (by volume) approximately 90% phlogopite, 4% clinohumite, 4% ore minerals (predominantly galena, arsenopyrite, pyrrohite and pyrite) and 2% diopside. Accessory minerals amounting to less than 1% are apatite, baryte, allanite-(Ce) and rare baddeleyite. Yttrian zirconolite accounts for approximately only 0.1 modal percentage, and occurs as anhedral grains predominantly 20–30 μm in size, and occasionally up to 60 μm. It is invariably observed as isolated grains associated with, and between phlogopite crystals and in backscattered electron images shows signs of secondary alteration and corrosion (Fig. 1*a,b*). In transmitted light zirconolite is predominantly yellow in colour, and in a few cases, has irregular dark brown domains. In reflected light, it has a similar appearance to sphalerite but is distinguished from sphalerite by having lighter and more intense internal reflections.

Chemical analyses were performed on electron microprobes in both Amsterdam and London, and a comparison of the results showed them to be in excellent agreement. The analysis was duplicated because first results (at Amsterdam) produced low analytical totals suggesting the presence of several wt.% of unanalysed element(s) other than oxygen. After repolishing and recoating the sample, two further analytical runs were made in London on 18 grains which confirmed the low totals of 94–95 wt.% oxide, with no other elements observed on either energy-dispersive, or wavelength-dispersive spectral scans. Similar low totals have been observed for zirconolites on two previous occasions: Borodin *et al.* (1960) who measured up to 5.66% H_2O in zirconolite from Alden, USSR, and Platt *et al.* (1987) who inferred the presence of several wt.% H_2O in zirconolite from Malawi. The Koberg zirconolite described here has a similar relatively light colour to that of previously reported hydrated zirconolites, and by analogy with them, the unanalysed 5–6 wt.% is considered also to be H_2O.

The presence of significant amounts of H_2O in zirconolite is unusual, and from the previous two occurrences cited above, appears to result from a

secondary hydration process related to fissioning of the actinide elements producing short-range disruption to the crystal lattice and thereby increasing its susceptibility to alteration (Platt *et al.*, 1987). This feature has important implications to radioactive waste management, since

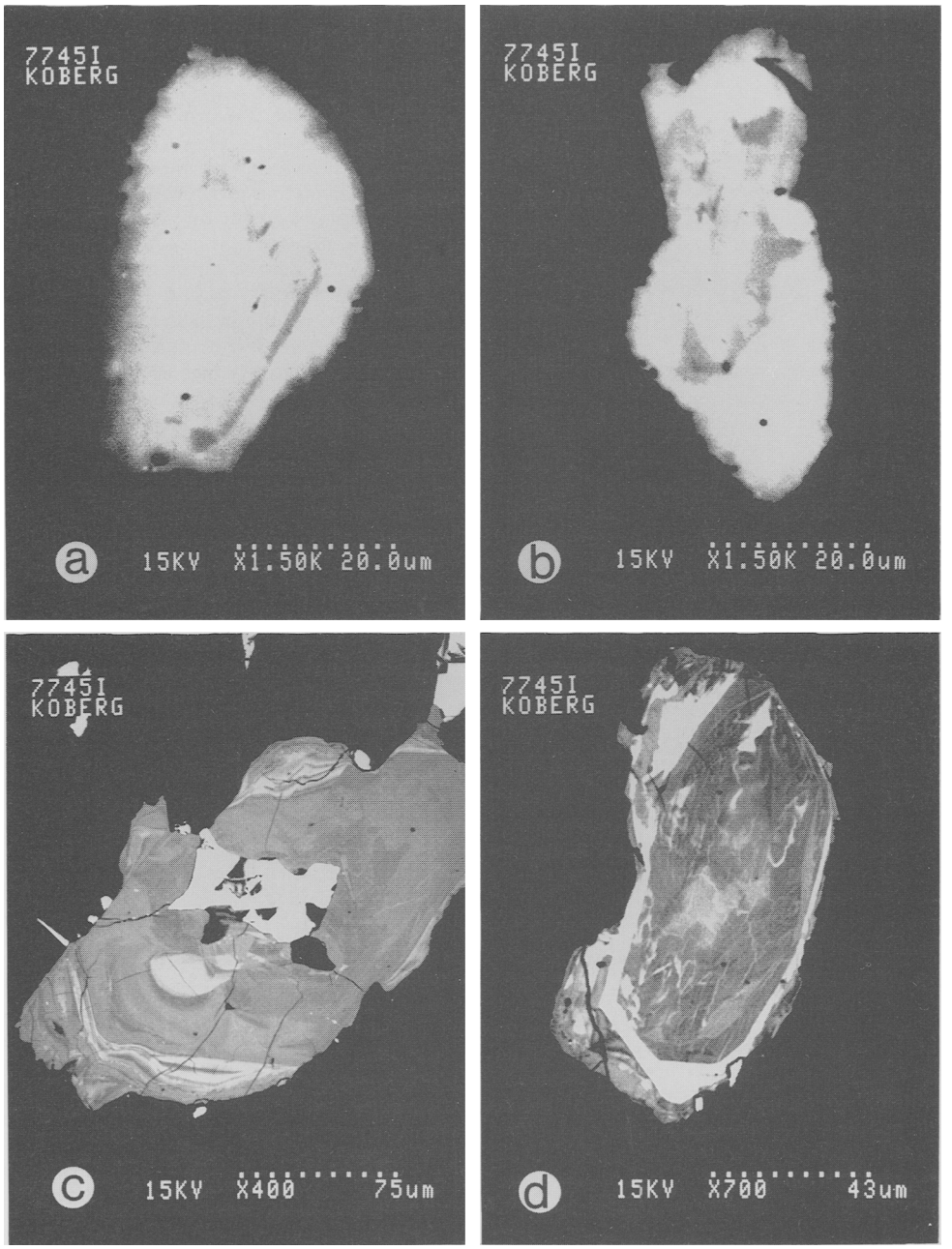

FIG. 1. (*a*), (*b*) are backscattered electron images of yttrian zirconolite. The lighter (higher mean atomic number) areas are enriched in actinide elements (Th and U) relative to the darker areas. (*c*), (*d*) are backscattered electron images of allanite-(Ce). The lighter areas and rims are enriched in $\Sigma(Y + REE_2O_3)$. The central white area in Fig. 1(*c*) is a sphalerite crystal.

Table 1. Microprobe analyses of yttrian zirconolite

	Mean	standard deviation σ_{n-1}	HA	HB
MgO	0.42	0.26	0.21	0.32
Al_2O_3	0.30	0.14	0.26	0.28
SiO_2	0.34	0.22	0.19	0.26
CaO	7.67	0.53	8.99	7.52
TiO_2	27.40	0.74	29.01	27.36
MnO	0.85	0.35	0.59	0.79
FeO	6.20	0.96	6.54	6.36
ZnO	0.55	-	-	-
Y_2O_3	4.64	0.63	3.22	4.58
ZrO_2	29.22	0.56	29.92	28.66
Nb_2O_5	2.82	0.60	2.10	2.76
La_2O_3	0.17	0.07	0.25	0.14
Ce_2O_3	1.80	0.46	2.69	1.68
Pr_2O_3	0.36	0.11	0.45	0.29
Nd_2O_3	3.08	0.23	3.31	3.09
Sm_2O_3	1.15	0.16	0.94	1.14
Gd_2O_3	1.31	0.19	0.87	1.28
Dy_2O_3	0.96	0.16	0.53	0.96
Er_2O_3	0.44	0.08	0.25	0.51
Yb_2O_3	0.37	0.10	0.23	0.42
HfO_2	0.79	0.15	1.04	0.51
Ta_2O_5	<.15	-	<.15	<.15
WO_3	0.44	0.21	0.78	0.37
PbO	0.26	0.18	<.10	0.29
ThO_2	1.69	0.55	0.74	1.78
UO_2	1.19	0.55	0.37	1.21
TOTAL	94.42	-	93.48	92.56
$(Y+REE)_2O_3$	14.28	0.73	12.74	14.09
Ca+2	0.574	0.038	0.666	0.573
Y+3	0.173	0.024	0.118	0.173
La+3	0.004	0.002	0.006	0.004
Ce+3	0.046	0.012	0.068	0.044
Pr+3	0.009	0.003	0.011	0.008
Nd+3	0.077	0.006	0.082	0.079
Sm+3	0.028	0.004	0.022	0.028
Gd+3	0.030	0.004	0.020	0.030
Dy+3	0.022	0.004	0.012	0.022
Er+3	0.010	0.002	0.005	0.011
Yb+3	0.008	0.002	0.005	0.009
Pb+2	0.005	0.003	0.000	0.006
Th+4	0.027	0.010	0.012	0.029
U+4	0.019	0.009	0.006	0.019
SUM Ca2+	1.032	-	1.034	1.035
Zr+4	0.996	0.015	1.009	0.995
Hf+4	0.016	0.003	0.021	0.010
SUM Zr4+	1.012	-	1.029	1.005
Mg+2	0.044	0.027	0.022	0.034
Al+3	0.025	0.011	0.021	0.023
Si+4	0.024	0.015	0.013	0.019
Ti+4	1.440	0.027	1.508	1.464
Mn+2	0.050	0.021	0.035	0.048
Fe+2	0.362	0.055	0.378	0.379
Zn+2	0.028	-	-	-
Nb+5	0.089	0.048	0.066	0.089
Ta+5	0.000	-	0.000	0.000
W+6	0.008	0.004	0.014	0.007
SUM Ti4+	2.070	-	2.057	2.062
TOTAL	4.114	-	4.120	4.102
O-2	7.000	-	7.000	7.000
Y+REE3+	0.399	-	0.350	0.408

Mean and standard deviation calculated from a total of 28 spot analyses on 18 grains. HA and HB are single spot analyses of one grain.
ZnO value is from a single analysis from the Amsterdam microprobe.

zirconolite is a major component in SYNROC which is proposed as a long-term storage and immobilization of high-level radioactive waste (e.g. Ringwood, 1985). Evidence for alteration of zirconolite in some geological environments therefore questions the efficacy of zirconolite-based radioactive waste repositories (see also Gieré and Williams, 1991).

The analytical data presented here for the Koberg zirconolite-(Y) was obtained using a Cambridge Instruments Microscan 9 wavelength-dispersive electron microprobe using the analytical conditions given by Williams and Gieré (1988). A total of 28 spot analyses were performed on 18 grains for which the mean and standard deviation (σ_{n-1}) are presented in Table 1. The complete analytical data set can be obtained on request from either MZ or CTW. Of note are the relatively high contents of MnO and $\Sigma(Y + REE_2O_3)$, and low analytical totals. The standard deviations are low for the major elements Ca, Ti, Zr and $\Sigma(Y + REE)$, but relatively high for the actinide elements Th and U. Actinide concentration vary, ranging from 1.10 to 4.62 wt.% $ThO_2 + UO_2$, and correlate with the patchy zoning observed in the backscatter electron images of Fig. 1*a* and *b*; the brighter regions are enriched in the actinide elements. Large variations in both Th and U have been observed in other metasomatic zirconolites from marble skarns (Williams and Gieré, 1988; Gieré, 1990).

Although $\Sigma(Y + REE_2O_3)$ values are relatively constant both from grain to grain, and within single grains, there are significant differences in some of the *REE*, in particular Y and Ce. Microprobe spot analyses from a single grain (HA and HB, Table 1) are plotted in the chondrite-normalized diagram, Fig. 2, and show a change had occurred from a relatively light-*REE* enriched pattern (HA) to a relatively heavy-*REE* enriched pattern (HB), pivoting about the position at Nd. A plot of Y_2O_3 against Ce_2O_3 for all the analytical data, Fig. 3, shows a reasonably good correlation between these element pairs, indicating that a significant degree of light- to heavy-*REE* fractionation had occurred at some stage of the zirconolite growth history, or during its subsequent alteration. It is noteworthy that this fractionation, manifesting in the chemical zoning, was not apparent in either optical microscopy or backscattered electron imagery.

The overall abundance of $\Sigma(Y + REE_2O_3)$ (14.28 ± 0.73 wt.% oxide) is relatively high compared with abundances from most other terrestrial zirconolites, but comparable with abundances of metasomatic zirconolites reported

from Bergell, Switzerland (Williams and Gieré, 1988) and Adamello, Itly (Gieré, 1990). The chondrite-normalized *REE* pattern however, is more similar to zirconolites from a gabbroic pegmatite from St. Kilda, Scotland, and to lunar zirconolites (Fowler and Williams, 1986).

Allanite-(Ce). Within the same sample as yttrian zirconolite, several large, up to 200 μm in size, grains of allanite-(Ce) were identified. Optically, the allanite is pale yellow in transmitted light, with minor pleochroism and is anisotropic, the low U and Th contents probably being insufficient for complete metamictization. It is often found associated and intergrown with sphalerite. Backscattered electron images show the grains are generally homogenous in composition, with the exception of thin (1–3 μm wide) zones and regions of higher mean atomic number (high-Z) component usually occurring towards the edges of the grains and following crystal outlines, Fig. 1*c,d*. Several microprobe spot analyses were made of three grains, two of which contained such high-Z zones. The results are presented in Table 2, together with the cations calculated on the basis of 12.5 oxygens following the procedure of Deer *et al.* (1986). Fe^{total} was distributed between Fe^{2+} and Fe^{3+} using the following procedure: firstly Fe^{3+} was calculated as $2 - Al^{3+}$; secondly Fe^{2+} was calculated from $Fe^{total} - Fe^{3+}$.

From Table 2, it can be seen that there are significant differences between the areas of the crystals, both in the chemistry and the degree of conformity to the allanite structural formula. The homogeneous areas comprising the bulk of the grains conform well with the structural formula. However, the high-Z areas are enriched in $\Sigma(Y + REE_2O_3)$ and depleted in all other major elements analysed, and do not conform well with the allanite structural formula. It is noteworthy also that low analytical totals were recorded from these zones. There are several reported occurrences of allanite altering to bastnäsite (e.g. Deer *et al.*, 1986), and it is postulated that the analyses

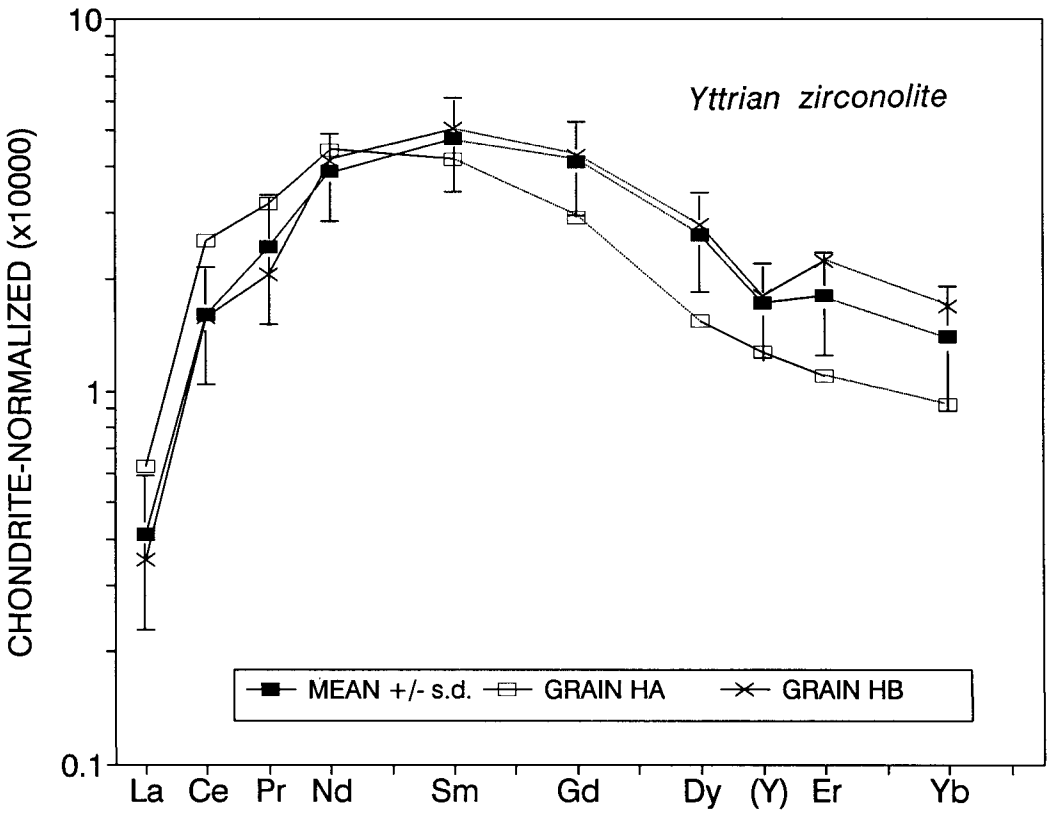

FIG. 2. Chondrite-normalized *REE* plots of the mean ± standard deviation of yttrian zirconolite, together with plots for Ce-rich, Y-poor (HA) and Ce-poor, Y-rich (HB) spot analyses from a single grain, illustrating pivoting of the chondrite-normalized pattern, within the grain, about the position at Nd.

of the high-Z areas in Table 2 correspond to submicron intergrowths of allanite plus a bastnäsite-type mineral. Although differences of 6–8% $\Sigma(Y + REE_2O_3)$ exist between the bulk allanite and the high-Z areas, the chondrite-normalized patterns are identical (Fig. 4), being both light-*REE* enriched and having a pattern quite distinct from the other rare earth mineral present, yttrian zirconolite.

The chemical composition of the bulk allanite is unusually rich in MgO, Table 2. Such high abundances of MgO have only been reported from the cerium mineral occurrences of the Bastnäs type of Central Sweden, where Geijer (1927) reports both a Mg-rich orthite containing 7.42% MgO and a magnesium orthite with 14.15% MgO. A comparison of these data with the Mg-rich allanite described here, Table 2, shows the Koberg allanite to be similar in composition to the Mg-rich orthite from Norberg. In addition to Mg-rich allanite, the associated mineral assemblage at Koberg includes tremolite, chondrodite, pyrope-garnet, molybdenite and sulphides within a dolomite and limestone skarn. This mineral assemblage is similar to that described by Geijer (1961) for the cerium deposits of Central Sweden.

Discussion

From textural relationships, zircon, baddeleyite and ilmenite are considered to be primary constituents of the exhalative–sedimentary sulphide ores of Koberg. The presence of yttrian zirconolite in fracture-filling phlogopite-rich rock ('sköl') associated with marble suggests a metasomatic origin for this mineral with the localized remobilization of Ti and Zr, from zircon, baddeleyite and ilmenite, in fluids enriched in H_2O and CO_2. The remaining mineral assemblage at Koberg including olivine, phlogopite, titanian clinohumite, apatite, zincian spinel and sulphides is closely similar to assemblages of metasomatic zirconolites from Switzerland and Italy (Gieré, 1986, 1990), produced by the interaction of fluid from an intrusion of interme-

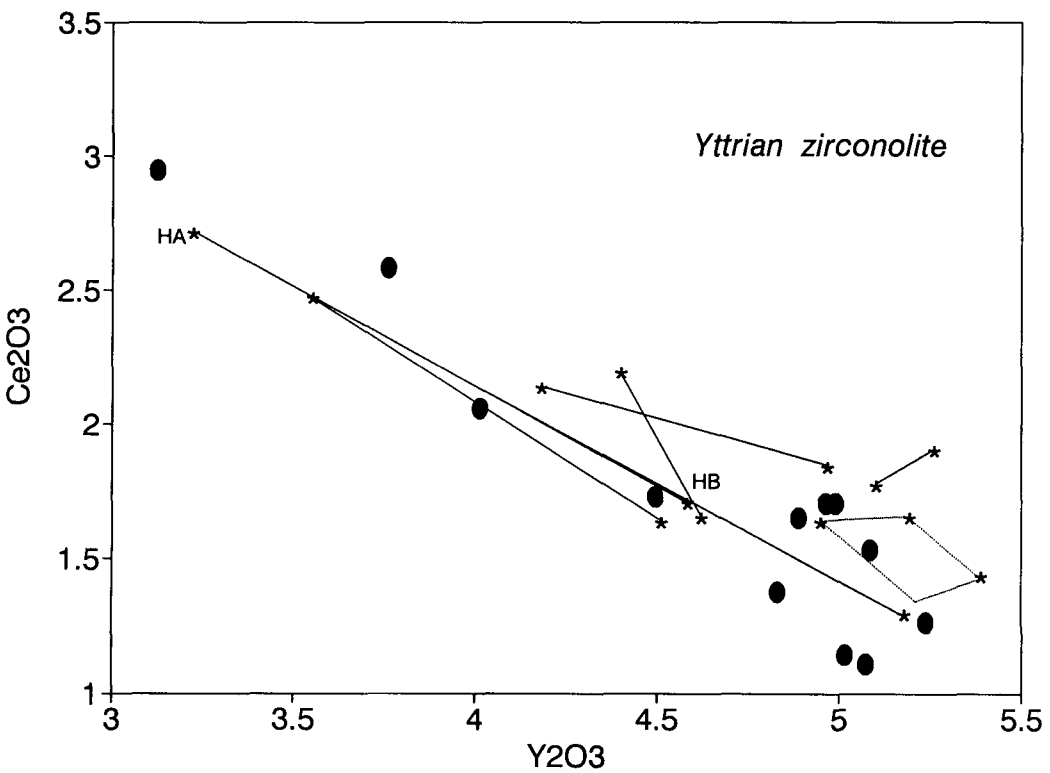

FIG. 3. Plot of Ce_2O_3 against Y_2O_3 for all microprobe analyses. Tie lines join data from single crystals, and illustrates the relatively good correlation of these elements both inter- and intra-crystals.

Table 2. Microprobe analyses of allanite-(Ce)

	1	2	3	4	5	6	7
MgO	5.84	5.28	5.20	3.01	3.48	7.42	14.15
Al_2O_3	14.47	15.50	15.62	10.66	10.74	10.09	8.05
SiO_2	32.48	33.18	33.00	28.08	28.10	31.85	31.39
CaO	10.66	11.19	11.23	8.32	8.56	9.57	9.36
TiO_2	0.62	0.51	0.51	0.60	0.57	0.02	0.01
MnO	0.29	0.32	0.32	0.39	0.43	0.27	0.50
FeO	0.96	2.01	2.23	0.00	0.30	5.34	2.29
Fe_2O_3	5.62	4.40	4.13	8.19	8.48	5.83	1.12
Y_2O_3	0.05	0.05	0.05	0.04	0.05	-	-
La_2O_3	7.95	7.69	8.03	10.86	9.98	15.50	17.00
Ce_2O_3	12.93	12.32	12.01	15.95	15.17	11.66	12.10
Pr_2O_3	1.10	1.09	1.06	1.56	1.44	-	-
Nd_2O_3	3.36	3.26	3.19	4.25	4.28	-	-
Sm_2O_3	<.2	<.2	<.2	0.27	0.25	-	-
Gd_2O_3	<.2	<.2	<.2	<.2	<.2	-	-
Dy_2O_3	<.2	<.2	<.2	<.2	<.2	-	-
ThO_2	0.25	0.22	0.32	0.42	0.32	-	-
UO_2	<.1	<.1	<.1	<.1	<.1	-	-
F	-	-	-	-	-	0.87	3.31
H_2O	-	-	-	-	-	1.79	2.02
TOTAL	96.02	95.11	96.48	91.78	91.29	100.21	101.30
$\sum(Y+REE)_2O_3$	25.39	24.41	24.34	32.94	31.17	27.16	29.20
Si	3.052	3.077	3.068	2.996	2.981	2.947	2.917
Al	0.000	0.000	0.000	0.000	0.019	0.053	0.083
$\sum$Si+Al	3.052	3.077	3.068	2.996	3.000	3.000	3.000
Al	1.602	1.694	1.711	1.341	1.324	1.047	0.799
Fe3+	0.397	0.307	0.289	0.658	0.677	0.406	0.078
$\sum$Al+Fe3+	1.999	2.001	2.000	1.999	2.001	1.453	0.877
Ti	0.044	0.036	0.036	0.048	0.045	0.001	0.000
Mg	0.818	0.730	0.721	0.479	0.550	1.023	1.960
Fe2+	0.076	0.156	0.173	0.000	0.026	0.413	0.178
$\sum$Mg+Fe2+	0.938	0.921	0.929	0.527	0.621	1.437	2.138
Mn	0.023	0.025	0.025	0.035	0.039	0.021	0.039
Ca	1.073	1.112	1.118	0.951	0.973	0.949	0.932
Y	0.002	0.002	0.002	0.002	0.003	-	-
La	0.275	0.263	0.275	0.427	0.390	0.529	0.583
Ce	0.445	0.418	0.409	0.623	0.589	0.395	0.412
Pr	0.038	0.037	0.036	0.061	0.056	-	-
Nd	0.113	0.108	0.106	0.162	0.162	-	-
Sm	0.000	0.000	0.000	0.010	0.009	-	-
Gd	0.000	0.000	0.000	0.000	0.000	-	-
Dy	0.000	0.000	0.000	0.000	0.000	-	-
Th	0.005	0.005	0.007	0.010	0.008	-	-
U	0.000	0.000	0.000	0.000	0.000	-	-
$\sum$Ca+REE	1.975	1.970	1.979	2.282	2.229	1.894	1.966
F	-	-	-	-	-	0.255	0.973
H	-	-	-	-	-	1.105	1.252
Total	7.963	7.969	7.967	7.804	7.851	9.114	10.205
$\sum$Y+REE3+	0.873	0.828	0.828	1.285	1.209	0.924	0.995

Analysis 1. Average of 4 spots - grain H
Analysis 2. Average of 4 spots - grain G
Analysis 3. Average of 6 spots - grain I
Analysis 4. High-z area, average of 2 spots - grain H
Analysis 5. High-z area, average of 2 spots - grain G
Analysis 6. Orthite, Ostanmossa, anal. 1, p.11, Geijer, 1927.
Analysis 7. Mg-orthite, Ostanmossa, anal. 2, p.11, Geijer, 1927.

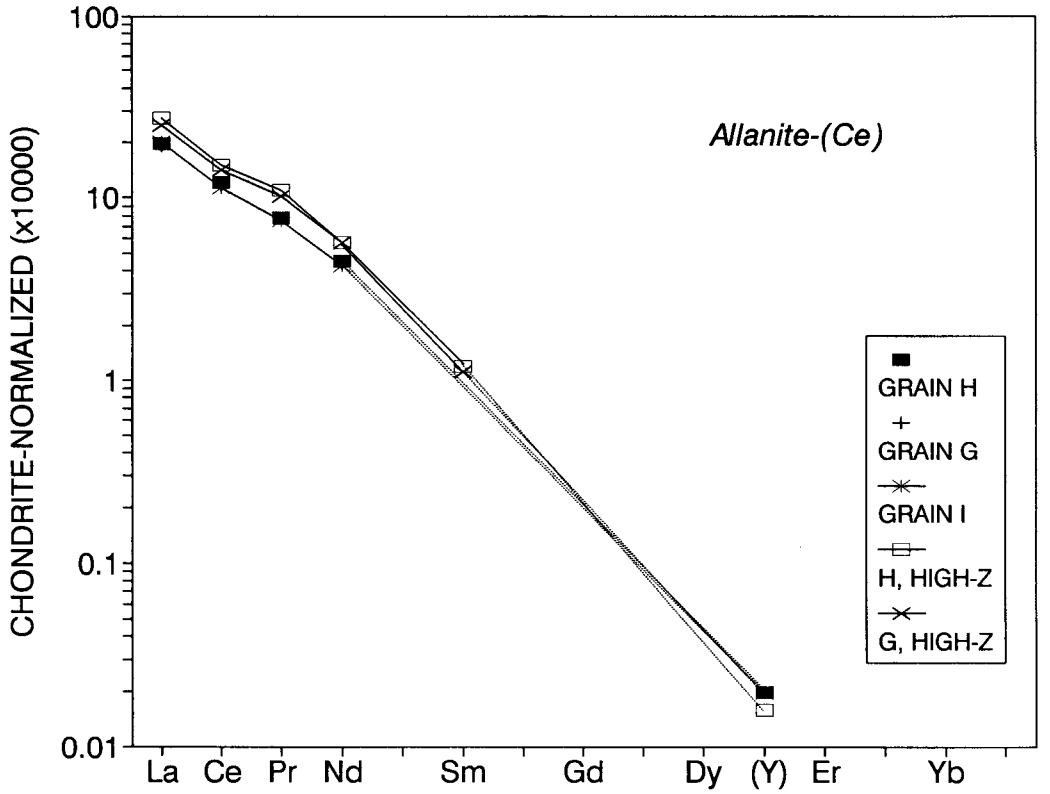

FIG. 4. Chondrite-normalized *REE* plot of allanite-(Ce) and the *REE*-rich zones within the allanite crystals. The patterns are identical and are both steeply light-*REE* enriched, and contrast with the middle- to heavy-*REE* enriched patterns of yttrian zirconolite in Fig. 2.

diate (tonalite) composition with limestone. At Koberg, the presence of Mg-rich allanite-(Ce) links this deposit with the cerium mineral deposits of Central Sweden described by Geijer (1961). Geijer (1927, 1961) interprets the high MgO contents to be the result of regional 'magnesia metasomatism' related to granitic emplacements, although the source of Mg is now considered to be the result of dedolomitization (e.g. Gavelin, 1989) or sea-water interaction (Baker *et al.*, 1988). The minor rare earth mineralization at Koberg is related to, and contemporaneous with these cerium deposits, where the origin of the *REE* bearing fluids, although uncertain, is probably related to local hydrothermal systems restricted to narrow, structurally-controlled zones of high fluid flow (see e.g. Baker *et al.*, 1988).

Summary and conclusions

(1) Coexisting rare earth minerals yttrian zirconolite and allanite-(Ce) were identified in mine dump samples from Koberg mine, Bergslagen, Sweden.

(2) Yttrian zirconolite is considered to be hydrated, with up to 6 wt.% H_2O present. The mineral is enriched in MnO, and additionally contains significant amounts of ZnO and WO_3.

(3) Actinide elements (Th and U) occur at minor concentration levels in yttrian zirconolite, and correlated with patchy zoning observed in back-scatter electron images.

(4) Although the $\Sigma(Y + REE_2O_3)$ in yttrian zirconolite is relatively constant, zoning is present in some individual *REE*, particularly Ce and Y.

(5) The mineral assemblage at Koberg is similar to that of other zirconolite-bearing metasomatic skarns, but the chemical composition of the zirconolites differ in some respects.

(6) Allanite-(Ce) contains an unusually high concentration of MgO, and is chemically similar to allanite (orthite) reported from several cerium mineral occurrences of Central Sweden.

(7) Minor *REE*-rich zones occur within allanite-(Ce) crystals, and it is considered that these zones

are sub-micron intergrowths of allanite with a bastnäsite-type mineral phase.

Acknowledgements

Electron microprobe facilities at Amsterdam were provided by the Free University (Amsterdam) and by WACOM, a working group for analytical geochemistry subsidized by The Netherlands Organization for the Advancement of Pure Research (NWO).

References

Baker, J. H., Hellingwerf, R. H., and Oen, I. S. (1988) *Geol. Mijnb.*, **67**, 121–38.

Bayliss, P., Mazzi, F., Munno, R., and White, T. J. (1989) *Mineral. Mag.*, **53**, 565–9.

Borodin, L. S., Bykova, A. B., Kapitonova, T. A., and Pyatenko, Yu. A. (1960) *Dokl. Acad. Sci. USSR, Earth Sci. Sect.*, **134**, 1022–4.

Deer, W. A., Howie, R. A., and Zussman, J. (1986) *Rock-forming Minerals*, 2nd ed., Vol. 1B, 151–79. Longman Scientific & Technical..

Fowler, M. B. and Williams, C. T. (1986) *Mineral. Mag.*, **50**, 326–8.

Frondel, J. W. (1975) *Lunar Mineralogy*, 323. New York, Wiley Interscience.

Gavelin, S. (1989) *Geol. Fören. Stockh. Förh.* **111**, 213–27.

Geijer, P. (1927) *Sver. Geol. Unders.*, Ser. C, no. 343.

—— (1961) *Arkiv. Mineral. Geol.*, **3**, 99–105.

Gieré, R. (1986) *Contrib. Mineral. Petrol.*, **93**, 459–70.

—— (1990) *Terra Nova*, **2**, 60–7.

—— and Williams, C. T. (1991) Gac-MAC-SEG 16, Abstracts, May 1991, A44.

Igelström, L. J. (1871) *Mineralogisk Vägvisare i Wermland*. Filipstad.

Platt, R. G., Wall, F., Williams, C. T., and Woolley, A. R. (1987) *Mineral. Mag.*, **51**, 253–63.

Purtscheller, F. and Tessardi, R. (1985) Ibid., **49**, 523–9.

Ringwood, A. E. (1985) Ibid., **49**, 159–76.

Rickard, D. T. (1988) *Geol. Mijub.*, **67**, 139–55.

Tegengren, F. R. (1924) Sveriges ädlare malmer och bergwerk. *Sver. Geol. Unders.*, Ser. Ca, 17.

Williams, C. T. and Gieré, R. (1988) *Schweiz. Mineral. Petr. Mitt.*, **68**, 133–40.

[*Manuscript received 10 September 1989: revised 15 July 1991*]

Addendum

After the manuscript was accepted for publication, the description of a new mineral, dissakisite, the Mg-analogue of allanite was brought to our attention. (Grew, E. S., *et al.* 'Dissakisite-(Ce), a new member of the epidote group and the Mg-analogue of allanite-(Ce) from Antartica', *Amer. Mineral.*, **76**, 1990–7.) It is apparent that the chemistry, optical properties and mineral paragenesis of allanite-(Ce) described here from Koberg is similar to that of the new mineral dissakisite-(Ce).